Supporting Information

Particle Dynamics of Nanoplastics Suspended in Water with Soil Microparticles: Insights from Small Angle Neutron Scattering (SANS) and Ultra-SANS

Anton Astner [a], Sai Venkatesh Pingali, [b], Hugh O'Neill [b], Barbara Evans [b], Volker Urban [b], Kenneth Littrell [b], Douglas Hayes [a,*]

[a] The University of Tennessee, Biosystems Engineering and Soil Science, 2506 E J. Chapman Dr, Knoxville, TN 37996, United States of America

[b] Oak Ridge National Laboratory, 1 Bethel Valley Road, Oak Ridge, TN 37831, United States of America

* Corresponding author, e-mail: dhayes1@utk.edu

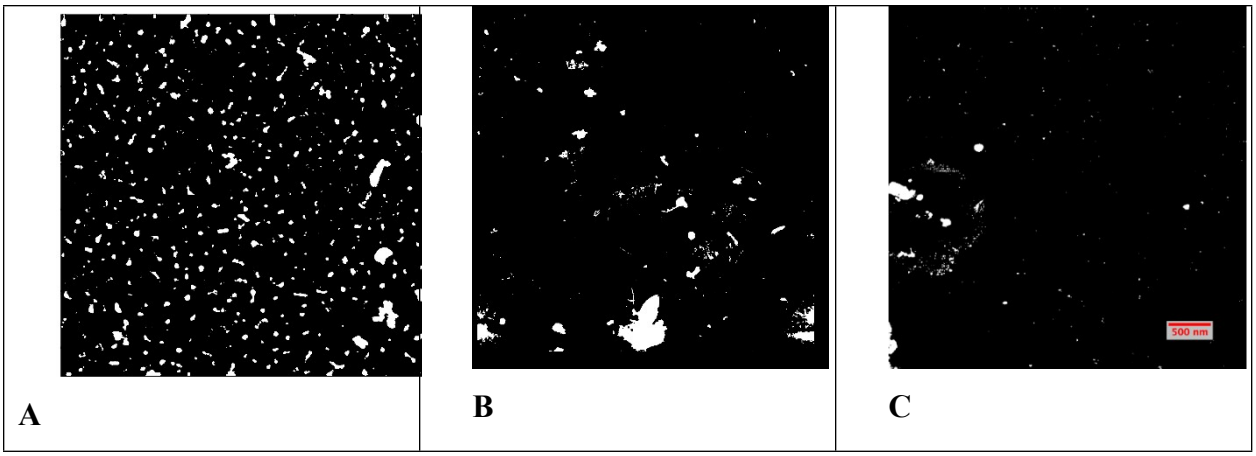

Fig. S1. Representative images of NPs obtained via atomic force microscopy (AFM), further processed using ImageJ software to improve the resolution of the NPs. **(A)** original NP batch prior to dispersing in water for the batch tests and SANS and USANS analyses. (**B)** and (**C):** bottom and top fractions (i.e., NPs that settled out of solution and remaining in solution after centrifugation, respectively) for NPs (1%) suspended in contrast match point (CMP) solvent, 67 (vol) % D_2O / 33% H_2O, for 168 hours of stirring. Scale given in **Fig. C** is applicable to **Figs. A. and B**.

The methodology for collecting AFM images is similar to the procedure described in our previous paper [1]. AFM images were prepared using a 4 µL aliquot of NP suspension in water that was deposited on a mica surface and air-dried for 1 h at room temperature (22±1°C) before scanning. For scanning the samples, a rectangular aluminum cantilever probe composed of an aluminum reflective coating on the backside was used. The AFM images were recorded on a scan area of 5.0 µm × 5.0 µm at a scanning speed of 1 Hz. For ImageJ analysis, the images were adjusted to 100 dpi = 1000 nm.

It is evident from **Fig. S1A** that NPs consist of a mixture of LNPs and SNPs, as described in our previous paper (Fig. S1 of the Supporting Information therein), and is devoid of SMPs to any significant extent [1]. It is also clear that NPs remaining suspended in solution possess a smaller size on average compared to the NPs that settle out of solution **(Figs. S1BC)**.

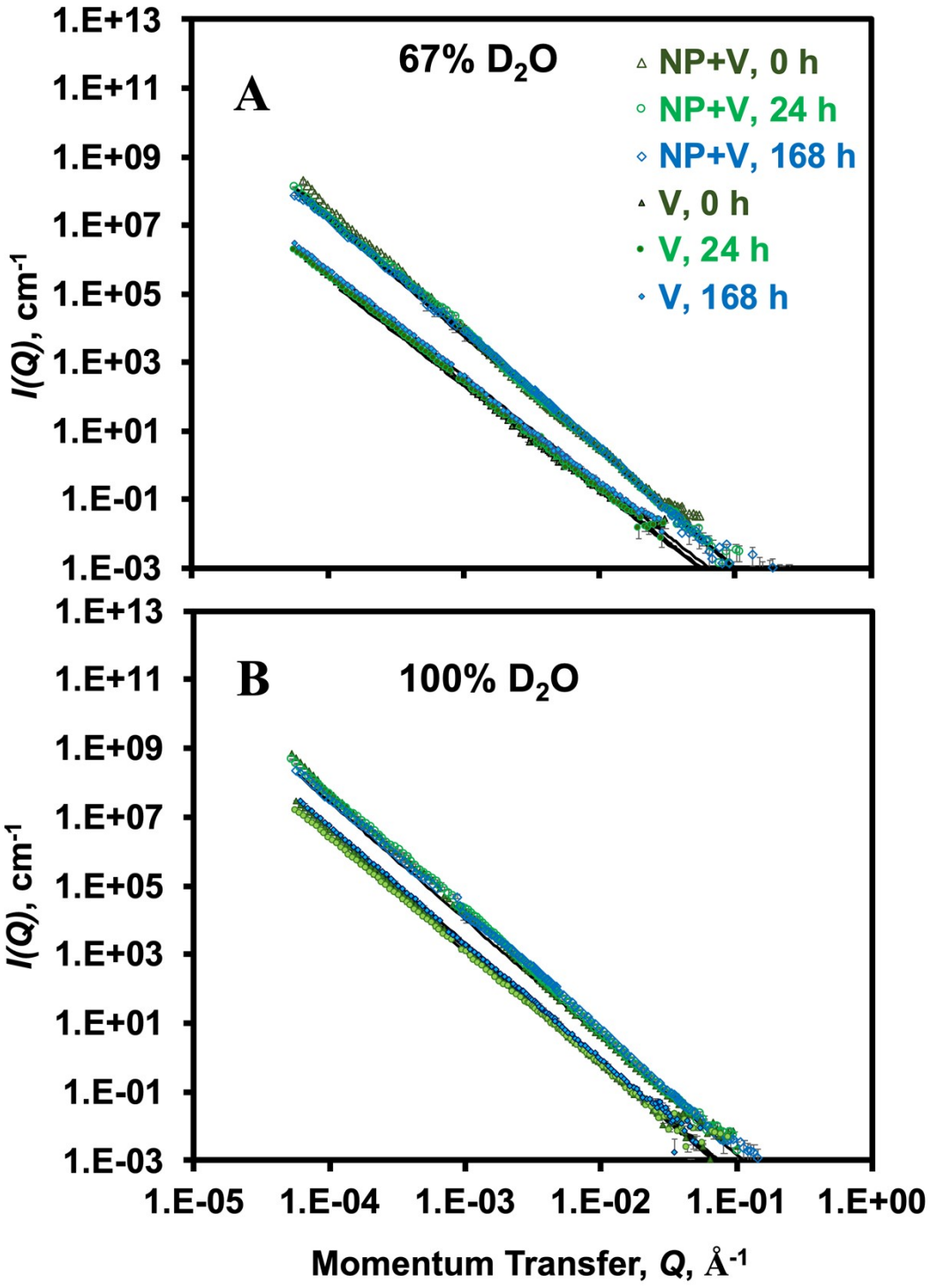

Fig. S2. Effect of *ex-situ* stirring time (0 h, 24 h, and 168 h) on merged SANS and USANS data for suspensions of PBAT NPs (1 wt%) and vermiculite (V) microparticles (0.5%) together and V alone (0.5%) in two solvents: **(A)** 67 vol% D_2O/33% H_2O (contrast match point, CMP, of V) and **(B)** 100% D_2O at 22°C.

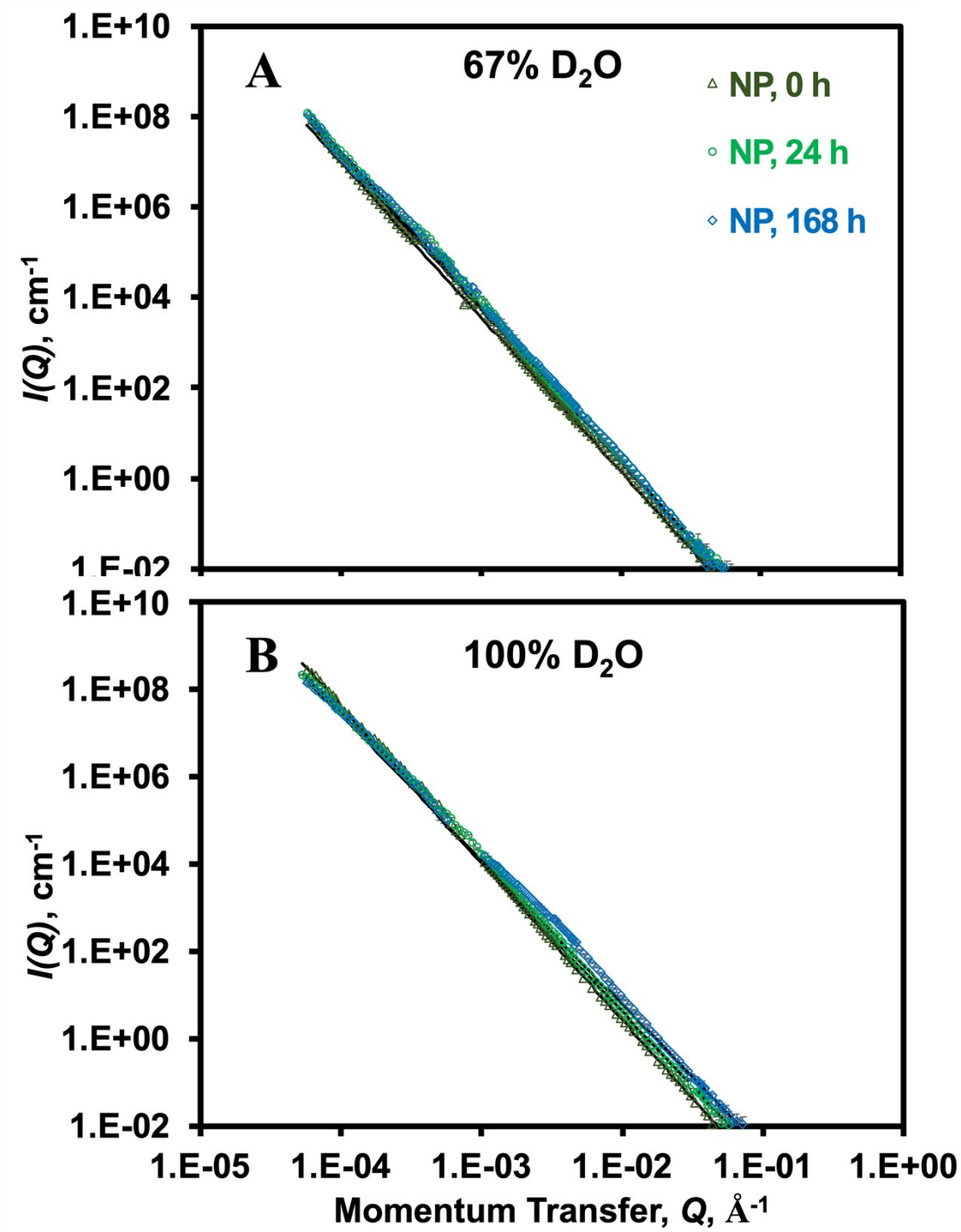

Fig. S3. Effect of *ex-situ* stirring time (0 h, 24 h, and 168 h) on merged SANS and USANS data for suspensions of PBAT NPs (1 wt%) in two solvents: **(A)** 67 vol% D_2O/33% H_2O (contrast match point, CMP, of V) and **(B)** 100% D_2O at 22°C. Error bars are smaller than the size of the symbols.

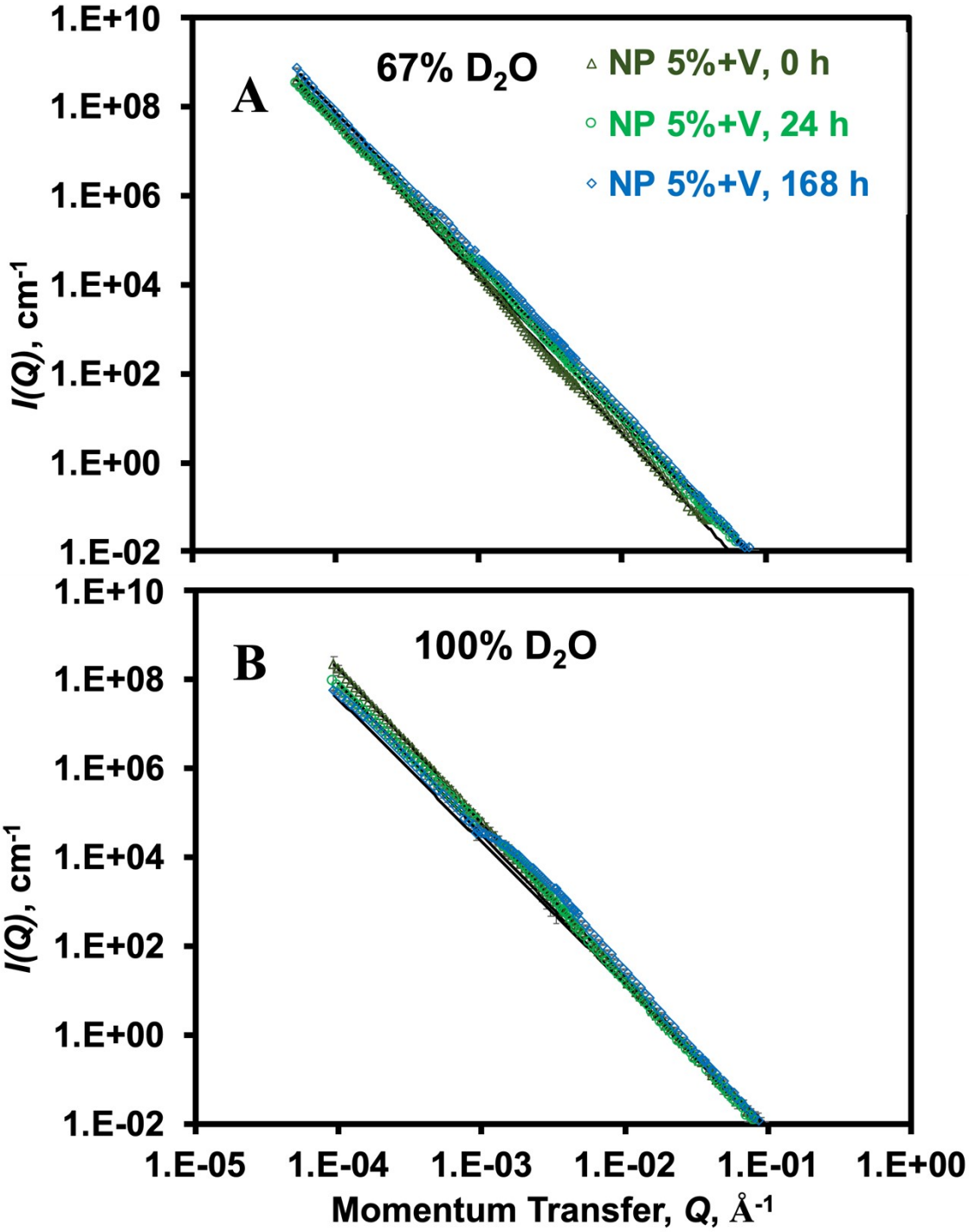

Fig. S4. Effect of *ex-situ* stirring time (0 h, 24 h, and 168 h) on merged SANS and USANS data for suspensions of PBAT NPs (5 wt%) and vermiculite (V; 0.5%) in two solvents: **(A)** 67 vol% D_2O/33% H_2O (contrast match point, CMP, of V) and **(B)** 100% D_2O at 22°C. Error bars are smaller than the size of the symbols.

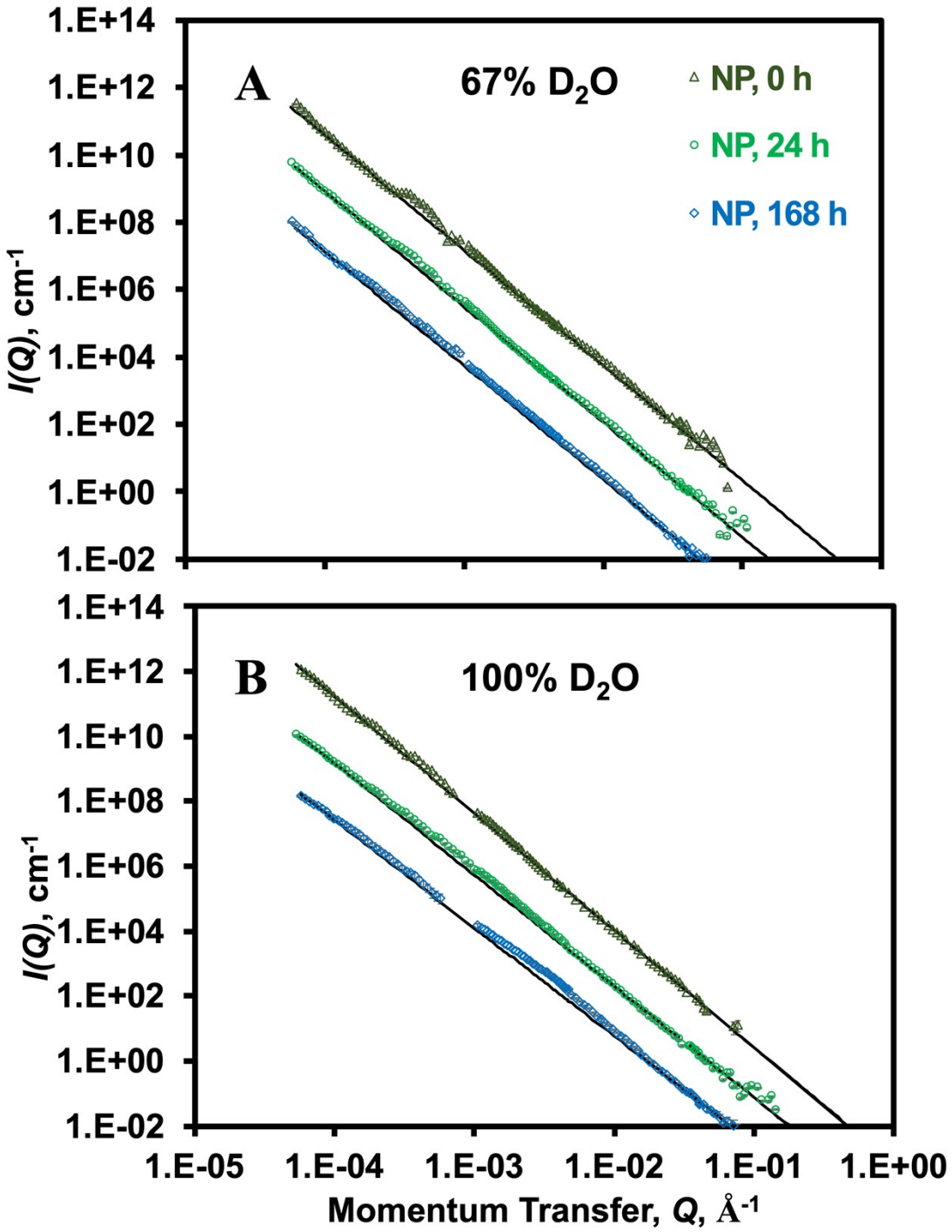

Fig S5. Fitting of Porod power law relationship (Eq. 2) to the merged SANS and USANS data depicted in Fig. S2. Effect of *ex-situ* stirring time (0 h, 24 h, 168 h) for PBAT NPs at 1 wt. %, suspended in **(A)** 67 % D_2O/33% H_2O (contrast match point of V) and **(B)** 100% D_2O at 22°C. For improved visualization, *I(Q)* data at 0 h and 24 h for **Figs. (A)** and **(B)** were multiplied by 4000 and 50, respectively.

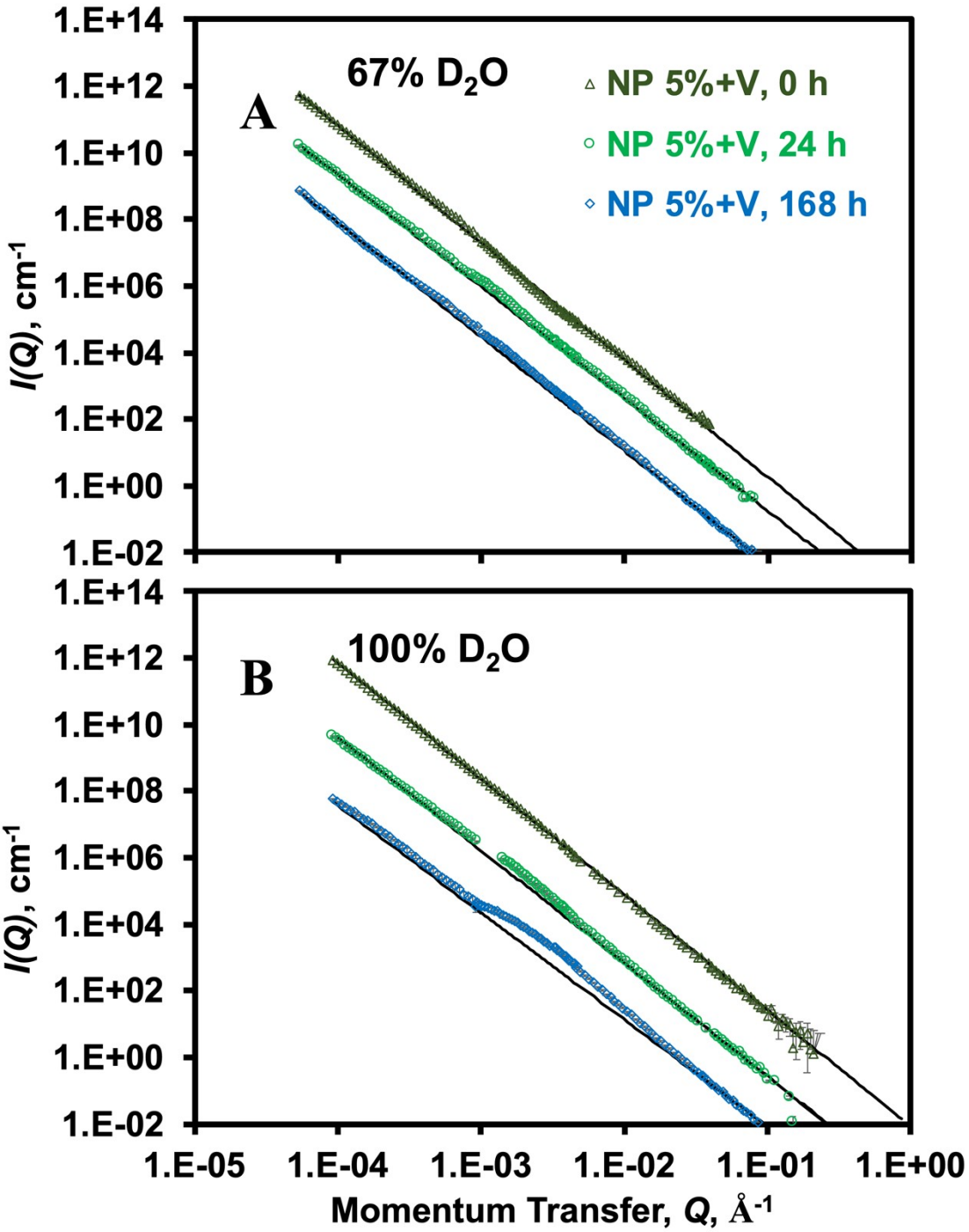

Fig. S6. Fitting of Porod power law relationship (Eq. 2) to the merged SANS and USANS data depicted in Fig. S4. Effect of *ex-situ* stirring time (0 h, 24 h, 168 h) for PBAT NPs and vermiculite (V) at 5 wt. % and 0.5%, respectively, suspended in **(A)** 67 % D_2O/33% H_2O (contrast match point of V) and **(B)** 100% D_2O at 22°C. To improve visualization, *I(Q)* data at 0 h and 24 h for **Fig. (A)** were multiplied by 4000 and 50, respectively, and for **Fig.** (**B)** by 150 and 15, respectively.

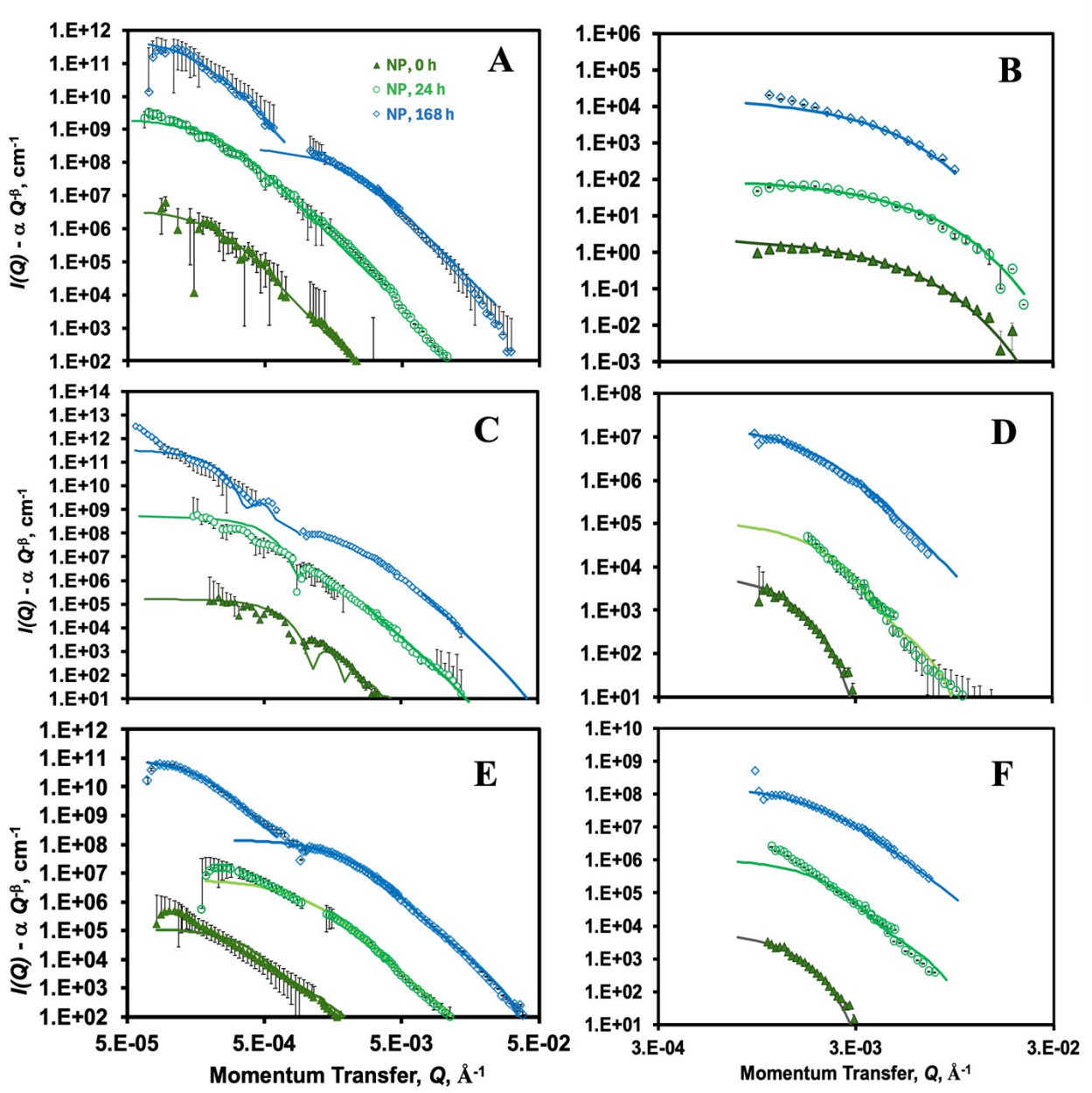

Fig. S7. Model fitting curves for oscillations for SANS and USANS scattering data after subtraction of the power law **(Eq. 2)** from *I(Q)* **(Figs. 2B, S5B, and S6B)** for suspensions of **(A, B)** NPs (1 %); **(C, D)** NPs (1%) + V (0.5%), and **(E, F)** NPs (5%) + V (0.5%) in 100% D_2O at 22°C. (**A, C, E)** USANS data fitted by a Schulz polydisperse sphere form factor model (**Eq. 4)** for large NPs (LNPs) and **(B, D, F)** SANS data fitted by a lognormal form factor model (**Eq. 3)** for small NPs (SNPs). Parameters derived from the model fitting and structure factors are presented in **Table 1**. USANS and SANS data for **Figs. A, C, and E** were multiplied by factors of 500 (24 h), and 50,000 (168 h), and for **Figs. B, D, and F** by factors of 50 (24 h) and 5,000 (168 h), respectively, to improve visualization.

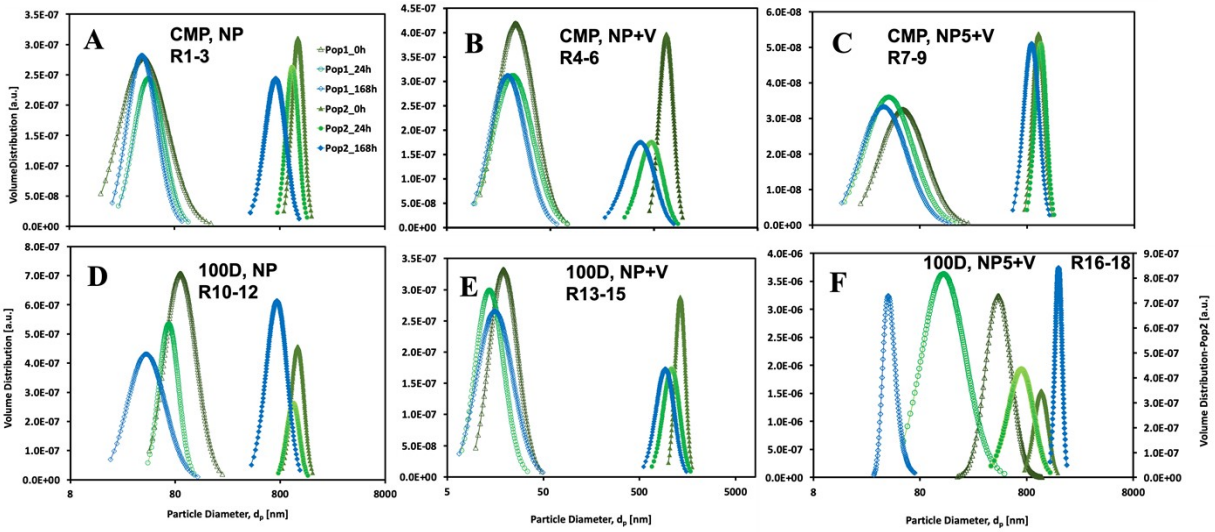

Fig. S8 (A) NP-Histograms of particle size distributions derived from the curve fitting provided by Igor and Irena software, which represents average particle size reduction because of *ex-situ* stirring. Smaller-sized nanoplastics (SNP) represent the lognormal fit and larger-sized NPs (LNPs) by polydisperse spheres (Schulz distribution). For **Fig. F**, the secondary y-axis corresponds to the three rightmost curves (LNPs).

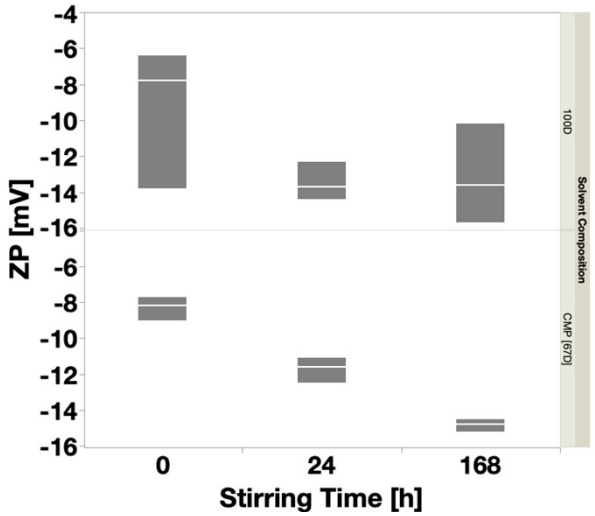

Fig. S9. Box plot of zeta potential of vermiculite (V; 0.5%) for CMP and 100% D_2O solvents vs *ex-situ* stir times. Instrumentation and approach are described in [2].

The data of **Fig. S8** support the main document's conclusions regarding how stirring time and solvent affect surface properties. For the CMP system (67% D_2O/33% H_2O), the zeta potential shifts from an average of about –8.3 mV at 0 hours to –14.8 mV at 168 h, indicating that prolonged stirring enhanced dispersion of V particles. This trend is consistent with the document's discussion of improved solvation and dispersion with increased stirring and for CMP solvent compared to

100% D_2O (Sect 4.5). Variation is much smaller for V suspended in CMP compared to 100% D_2O for the same reason. By comparison, the 100% D_2O samples show a higher variability and a slightly less marked change over time—averaging around –9.3 mV at time zero and –13.2 mV at 168 h.

Table S1. Parameters derived from the fit of the Porod power law (**Eq. 2**) to the merged SANS and USANS data, as shown in *Figs. 3, S5, and S6*

Suspended Particles [1]	***Ex-situ* Stir Time, h**	**Pre-Exponential Constant, log(α)**	**Power Law exponent, β**	**Surface fractal (*Ds*)** [2]
CMP (67% D_2O / 33% H_2O)				
NP (1%)	0	-6.71±0.019	3.42±0.006	2.58
NP (1%)	24	-6.46±0.013	3.42±0.004	2.58
NP (1%)	168	-6.40±0.022	3.38±0.007	2.62
NP (1%) + V	0	-6.41±0.020	3.47±0.006	2.53
NP (1%) + V	24	-6.44±0.014	3.43±0.004	2.57
NP (1%) + V	168	-6.34±0.027	3.37±0.008	2.63
NP (5%) + V	0	-6.74±0.015	3.49±0.004	2.51
NP (5%) + V	24	-5.82±0.013	3.37±0.004	2.63
NP (5%) + V	168	-5.80±0.021	3.42±0.008	2.58
V	0	-6.98±0.065	3.15±0.027	2.85
V	24	-6.80±0.037	3.07±0.016	2.93
V	168	-6.56±0.014	3.05±0.016	2.95
100% D_2O				
NP (1%)	0	-6.79±0.016	3.60±0.005	2.40
NP (1%)	24	-6.26±0.021	3.43±0.007	2.57
NP (1%)	168	-5.88±0.023	3.32±0.008	2.68
NP (1%) + V	0	-6.49±0.010	3.55±0.003	2.45
NP (1%) + V	24	-6.22±0.057	3.48±0.015	2.52
NP (1%) + V	168	-6.09±0.014	3.42±0.046	2.62
NP (5%) + V	0	-5.67±0.038	3.48±0.013	2.52
NP (5%) + V	24	-5.66±0.018	3.40±0.006	2.60
NP (5%) + V	168	-5.30±0.027	3.21±0.009	2.79
V	0	-6.91±0.028	3.36±0.012	2.64
V	24	-6.73±0.026	3.27±0.011	2.73
V	168	-6.47±0.019	3.37±0.008	2.63

[1] Vermiculite (V) concentration in aqueous suspension was 0.5 wt. %; [2] Ds = 6-β; Ds = 3 (β = 3) reflects a rough surface, while Ds = 2 (β = 4) represents a smooth surface for pores

Table S2. Comparison of the average volume fractions (ϕ) of NPs determined via SANS and USANS *(Table 1)* and through the batch experiments displayed in *Figure 1* [1]

Run Conditions [2]	ϕx10^4 (SANS + USANS) [3]	ϕx10^4 (Batch Tests) [4]	ϕx10^4 (SANS + USANS) [3]	ϕx10^4 (Batch Tests) [4]
Solvent	**CMP [5,6]**	**CMP [5]**	**D_2O [6]**	**D_2O**
1% NP, 0 h	5.19	2.63	4.17	6.84
1% NP, 24 h	7.30	3.48	28.6	9.44
1% NP, 168 h	6.42	7.90	21.5	11.2
1% NP+V, 0 h	8.62	4.16	52.6	1.61
1% NP+V, 24 h	8.47	7.22	25.8	8.11
1% NP+V, 168 h	12.4	10.2	13.7	11.7
5% NP+V, 0 h	3.92	14.0	30.2	1.98
5% NP+V, 24 h	10.6	42.5	13.0	5.49
5% NP+V, 168 h	12.1	49.7	16.1	7.60
0.5% V, 0 h	NA	2.97	NA	2.85
0.5% V, 24 h	NA	1.49	NA	2.36
0.5% V, 168 h	NA	0.99	NA	2.36

[1] It is assumed that the dispersed phase volume fraction, ϕ, is composed of 100% NPs and no V; [2] V refers to vermiculite (artificial soil), 0.5%; [3] determined by adding together ϕ for SNP and LNP, as determined by SANS form factor model fitting, but excluding the contribution of SMPs (*Table 1*); [4] determined from the percent recovery by mass values displayed in Table 1; [5] 67 (vol)% D_2O and 33% H_2O; [6] NA indicates not available, since no SANS or USANS oscillations occurred for 0.5% V.

Table S3. Settling velocity (v_s) for NPs and V in 67 (vol)% D_2O/33% H_2O (contrast match point, or CMP, solvent) and in 100% D_2O at 22^{o}C.

Solute	Solvent	v_s [1], m/s
(PBAT) NPs [2]	CMP [3]	1.51 x 10^{-9}
Vermiculite (V) [4]	CMP [3]	8.94 x 10^{-4}
(PBAT) NPs [2]	100% D_2O [5]	1.13 x 10^{-9}
Vermiculite (V) [4]	100% D_2O [5]	8.12 x 10^{-4}
(PBAT) NPs [2]	100% H_2O [6]	2.48 x 10^{-9}
Vermiculite (V) [4]	100% H_2O [6]	1.10 x 10^{-3}

[1] Calculated according to Stokes Law (assuming laminar flow conditions): $v_s = d_p^2 g(\rho_p - \rho_{solv})/18\mu$, where d_p is the particle diameter, g is the acceleration due to gravity, ρ_p the particle density, ρ_{solv} the solvent density, μ the viscosity of solvent; [2] ρ_p =1260 kg/m^3, d_p=132 nm; [3] ρ_{solv} =1070 kg/m^3, μ =1.17 x 10^{-3} Pa s; [4] ρ_p =2400 kg/m^3, d_p =38 mm; s; [5] ρ_{solv} =1100 kg/m^3, μ =1.25 x 10^{-3} Pa s. [6] ρ_{solv} =998 kg/m^3, μ =1.00 x 10^{-3} Pa

REFERENCES

1. A. F. Astner, D. G. Hayes, S. V. Pingali, H. M. O'Neill, K. C. Littrell, B. R. Evans and V. S. Urban, Effects of soil particles and convective transport on dispersion and aggregation of nanoplastics via small-angle neutron scattering (SANS) and ultra SANS (USANS), *PLoS One*, 2020, **15**, e0235893.

2. A. Astner, D. Hayes, H. O'Neill, B. Evans, S. Pingali, V. Urban, S. Schaeffer and T. Young, Assessment of cryogenic pretreatment for simulating environmental weathering in the formation of surrogate micro-and nanoplastics from agricultural mulch film, *Science of The Total Environment*, 2023, **870**, 161867.

3. Z. Wang, G. Wang, Z. Xu, C. Yang and G. Zhao, Structure-tunable poly (butylene adipate-co-terephthalate) foams with enhanced mechanical performance derived by microcellular foaming with carbon dioxide as blowing agents, *Journal of CO2 Utilization*, 2023, **72**, 102495.

4. J. Kestin, N. Imaishi, S. Nott, J. Nieuwoudt and J. Sengers, Viscosity of light and heavy water and their mixtures, *Physica A: Statistical Mechanics and its Applications*, 1985, **134**, 38-58.